Quantum-Teleportation-Inspired Algorithm for Sampling Large Random Quantum Circuits

Ming-Cheng Chen,[1,2] Riling Li,[3] Lin Gan,[3,4] Xiaobo Zhu,[1,2] Guangwen Yang,[3,4] Chao-Yang Lu,[1,2] and Jian-Wei Pan[1,2]

[1]*Hefei National Laboratory for Physical Sciences at Microscale and Department of Modern Physics, University of Science and Technology of China, Hefei, Anhui 230026, China*

[2]*CAS Centre for Excellence and Synergetic Innovation Centre in Quantum Information and Quantum Physics, University of Science and Technology of China, Hefei, Anhui 230026, China*

[3]*Department of Computer Science and Technology, Tsinghua University, Beijing 100084, China*

[4]*National Supercomputing Center in Wuxi, Jiangsu 214072, China*

(Received 24 July 2019; revised manuscript received 1 October 2019; accepted 7 February 2020; published 26 February 2020)

Quantum teleportation transfers and processes quantum information through quantum entanglement channels. It is one of the most versatile protocols in quantum information science and leads to many remarkable applications, particularly the one-way quantum computing. Here, we show, for the first time, that the concept of teleportation can also be used to facilitate an important classical computing task, sampling random quantum circuits, which is highly relevant to prove the near-term demonstration of quantum computational supremacy. In our method, the classical computation in the physical-qubit state space is converted to simulate teleportation in logical-qubit state space, resulting in a much smaller number of qubits involved in classical computing. We tested this new method on 1D and 2D lattices up to 1000 qubits. This Letter presents a new quantum-inspired classical computing technology and is helpful to design and optimize classically hard quantum sampling experiments.

DOI: 10.1103/PhysRevLett.124.080502

Information processing at a quantum mechanics level has attracted great scientific interest since the development of quantum polynomial time factoring algorithms and fault-tolerant quantum computing theory [1]. Many quantum algorithms are proposed to speed up solving important problems, such as solving linear systems [2] and complex molecular structures [3]. Recently, high-fidelity quantum gates above the fault-tolerance threshold have been demonstrated on superconducting qubits and trapped ions [4–6]. However, despite the great theoretical and experimental progress in the past two decades, these promising quantum algorithms still suffer from the lack of large-scale fault-tolerance quantum computing hardware or lack of strict proof of the computation complexity advantage.

The emerging quantum algorithms of quantum sampling offer a new opportunity to demonstrate quantum computation advantages in near-term quantum computing devices [7–10]. The argument from the computation complexity theory states that there is no efficient classical algorithm to simulate random quantum sampling unless the polynomial hierarchy collapses. Furthermore, the classically hard quantum sampling can be designed and implemented on near-term small-scale noisy quantum computers [11].

For example, boson sampling on linear optics systems [7] and random quantum circuit sampling on superconducting-qubit systems [12,13] are among the most promising candidates. According to the initial estimation, about 30 single-photon boson sampling [7] or 49-qubit quantum circuit sampling [12] will be beyond the simulation capabilities of state-of-the-art supercomputers.

However, the classical hardness of quantum sampling in computation complexity arguments is an asymptotic statement. Exactly how large of a size of quantum sampling problem will be enough to surpass classical computers is still subtle [14]. Recent progress in classical algorithms has broken the initial 49-qubit barrier by methods of tensor network contraction or modified Feynman-path summation [15–23]. An interesting question was naturally raised: where is the exact boundary of classical simulation? A physically intuitive answer to this question will help to design and optimize near-term quantum sampling experiments. In this Letter, we describe a quantum-teleportation-inspired classical method to solve large random quantum circuit sampling problems, where the traditional classical boundary of 49 physical qubits is updated to 49 logical qubits.

Classical simulation of quantum sampling includes two successive steps: (1) compute the probability amplitudes of some random candidate samples, and (2) choose effective samples according to the computed probability amplitudes. Step 1 is exponentially hard for classical computing due to the exponential scaling of the Hilbert space with the number of qubits. While step 2 is classically easy, its main point is to generate statistically independent samples with high sampling efficiency.

We begin to describe the computing of probability amplitude in step 1. A quantum circuit U_C is a sequence of quantum gate operations on a multiqubit quantum state. In the circuit, the quantum information, encoded in physical qubits, flows from the left to the right end. Given an input state $|0\rangle$ and a random output state $|i\rangle$, the circuit is equivalent to a complex number $\langle i|U_C|0\rangle$, called probability amplitudes.

A key observation is that the quantum circuit can also be interpreted as a quantum information flow diagram, where the lines in the circuit guide the flow of information. The lines include the world lines of physical qubits and the entangling lines of 2-qubit gates. As all the lines merely represent quantum correlations, quantum information can flow along the lines in an arbitrary direction. So, we can define new virtual logical qubits, starting from some ports of the circuit diagram, to redirect the information flow along the lines, while keeping the final probability amplitudes unchanged.

This concept is inspired by quantum-teleportation protocol [24,25], as illustrated in Fig. 1(a). The quantum-teleportation circuit has three physical qubits. A new logical qubit can be defined and used to redirect the information flow along the circuit topological structure, crossing the Bell measurement and Bell state, and then implement the quantum information transfer. This concept also reminds one of the one-way quantum computing, where the quantum information (logical qubits) flows along the cluster state of physical qubits. The key distinction in our protocol is the quantum information flows along the entangling gates without the underlying physical qubits.

A useful feature in our protocol is that the number of logical qubits can be much smaller than the physical qubits for a low-depth quantum circuit. We show the basic idea in Fig. 1(b), where the circuit consists of several layers of 2-qubit entangling gates. In this example, logical qubits are defined to flow transversely along the layers of entangling gates. Here, the roles of world lines of physical qubits and entangling lines of 2-qubit gates in the circuit are exchanged: the logical qubits exist on the entangling lines and they are entangled by the world lines. As the number of logical qubits is proportional to the circuits depth, the new circuit can be classically efficiently simulated when the number of logical qubits is below 49.

Our protocol can be explained as a Wick rotation on tensor network, which is a 90 deg rotation of a Feynman diagram of a quantum circuit amplitude [23]. The rotation globally exchanges the roles of space and time. In this setting, the quantum information is teleported along an imaginary time, and the space footprint of logical qubits determines the algorithm's memory space. The basic mathematical principle underlying the protocol is that a quantum gate circuit can be translated to a tensor network [26,27], and then the tensor network is translated back to a new quantum gate circuit. That is, two different quantum gate circuits can share the same tensor network. We show an example of circuit transformation in Fig. 1(c). Two key

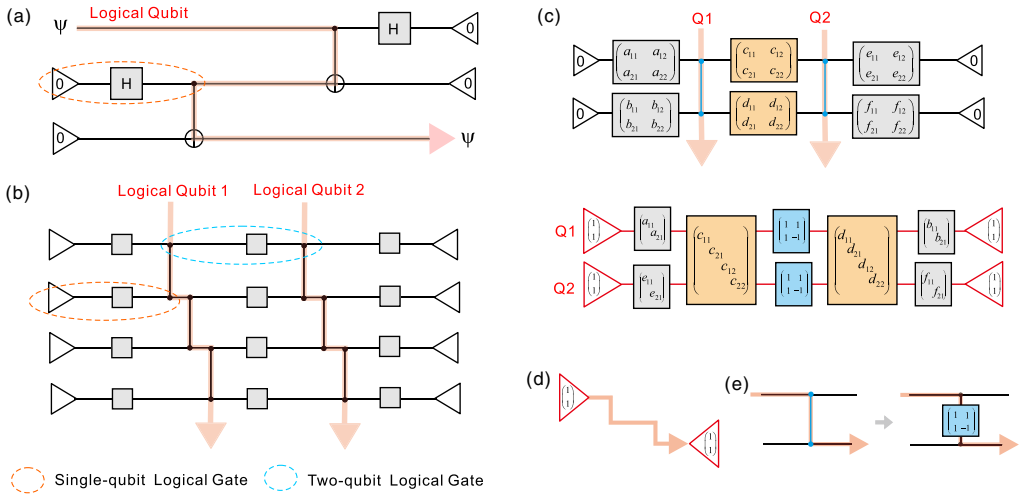

FIG. 1. Quantum-teleportation-inspired classical algorithm. (a) The circuit of quantum teleportation. Three physical qubits (black lines) in the quantum circuit are mimicked by one logical qubit (pink line). The logical qubit is used to redirect the flow of quantum information along the circuit topological structure. (b) Classical simulation of low-depth quantum circuits. Logical qubits are defined along the layers of 2-qubit entangling gates. The number of logical qubits is proportional to the circuits depth. For a low-depth circuit, the number of logical qubits can be far less than the physical qubits, therefore providing a memory-efficient classical simulation framework. (c) An example of circuit transformation from physical-qubit unitary circuit to logical-qubit-based nonunitary circuit. Nonunitary circuits can be directly simulated by matrix-vector multiplication. (d),(e) Two key circuit transformation widget. (d) A logical qubit begins from and ends at vector (1,1), respectively. (e) A diagonal 2-qubit gate on physical qubits is mapped into a single-qubit gate on a logical qubit.

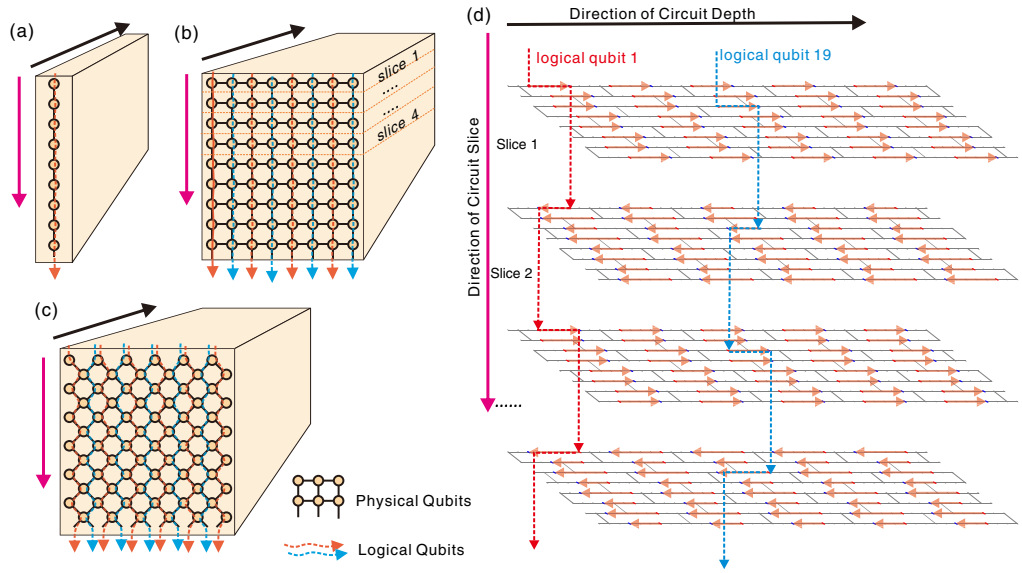

FIG. 2. Simulation of 1D and 2D random quantum circuits. (a)–(c) Quantum circuits are indicated by the volume of the yellow boxes. The lattice layouts of physical qubits are shown on the front surfaces of the boxes. The quantum information of the physical qubits flows along the direction of circuit depth and the quantum information of the defined logical qubits flows along the direction of circuit slices. (a) 1D quantum circuit with 1000 qubits and 42 depths. One logical qubit is defined for each circuit depth. (b) 2D quantum circuit with 125×8 qubits and 42 depths. Eight logical qubits are defined for every eight circuit depths. (c) Modified 2D quantum circuit with 12×6 qubits and 32 depths. Eleven logical qubits are defined for every eight circuit depths. (d) The layout of logical qubits for circuit (b). The world lines of physical qubits and entangling lines of 2-qubit gates inside the circuit slides are shown as gray lines. The entangling lines of 2-qubit gates across the circuit slices and all the single-qubit gates are not shown. The logical qubits flow inside the circuit slices (shown as red arrows) and across the circuit slices through the entangling gates between two neighboring slices (as shown as dashed lines).

transformation widgets are shown in Figs. 1(d) and 1(e) (see Supplemental Material [28] for other widgets).

Layer-structure circuits are the candidates for demonstrating quantum computational supremacy [12] and are hardware-efficient circuits for near-term quantum optimization application [29]. We demonstrate the protocol on three circuit examples, as shown in Fig. 2. In the first example [Fig. 2(a)], the qubits are arranged on a 1D lattice with nearest-neighbor interaction [30,31]. The circuit consists of alternating layers of random single-qubit gates and 2-qubit controlled-phase (CZ) gates. We define the logical qubits along the layers of CZ gates. Thus, an N-qubit and L-depth circuit is mapped into a new L logical qubit and N-depth circuit.

In the second example [Fig. 2(b)], the qubits are arranged on a 2D lattice with size $M \times N (M \geq N)$. The circuit consists of repetitive sparse patterns of CZ gates, where every 8 cycles of the patterns make each pair of the nearest-neighbor qubits entangle once (see Supplemental Material, Fig. S2 [28]). Meanwhile, random single-qubit gates are placed on some idle qubits in each cycle. This circuit has been proposed for demonstrating quantum computational supremacy with superconducting quantum circuits [12]. We define N logical qubits for every 8 circuit depths, and we transversely divided the circuit into M slices. The logical qubits go forward and backward on the world lines inside the slices and go across adjacent slices by the entangling lines (see Supplemental Material, Fig. S4 [28]), in the same style of the quantum-teleportation circuit in Fig. 1(a). Thus, an $M \times N$-qubit and $8 \times L$-depth circuit is mapped into a new $N \times L$ logical-qubit circuit, which is beneficial when $M > L$.

The third example is a modified version of the second example. The qubits are arranged on 2D lattice rotated by 45° with a diamond boundary [21] [Fig. 2(c), also see Supplemental Material [28], Figs. S3 and S5]. For an $M \times N (M \geq N)$ lattice, we define $2N - 1$ logical qubits for every 8 circuit depths. So, for an $M \times N$-qubit and $8 \times L$-depth circuit, the new circuit is of $(2N - 1) \times L$ logical qubits, which is beneficial when $(M \times N / 2N - 1) > L$.

We test the above examples on the supercomputer Sunway TaihuLight [32], which has 40 960 computing nodes and each node has 32 GB memory and 3 teraflops performance. The total memory is 1.25 PB, so a state vector of up to 48 logical qubits can be stored. We set the first circuit example with 1000 physical qubits and 42 depths, the second example with $M \times N = 125 \times 8$ qubits and 42 depths, and the third example with $M \times N = 12 \times 6$ qubits and 32 depths. The circuit simulation is based on the evolution of wave function according to the optimizations in our previous work [19]. The simulator uses 4096, 1024, and 16 384 computing nodes to produce a probability amplitude in 297.8, 131.6, and 14.1 min, respectively.

Next, we go to the subsequent step 2 to generate effective samples from the calculated probability amplitudes in

step 1. In general, it will consume several probability amplitudes to produce an effective sample. For example, Metropolis sampling using 100 probability amplitudes [33] and frugal rejection sampling using a batch of tens of probability amplitudes [21] are proposed to produce one sample.

Considering nonfault-tolerant quantum sampling devices are of finite fidelity, it is fairer for the classical algorithm to produce approximate samples in the task of sampling. Here, we describe a new sampling protocol for step 2, which has a sweet spot between the sampling efficiency and the sample fidelity.

The probabilities $\{p(i)|i = 0, 1, 2, \ldots, 2^n - 1\}$ of an n-qubit random quantum state at the output of random circuit obeys an exponential distribution [12]. After sorting the probabilities in ascending order, the function shape has a high and narrow peak and a long tail, that is,

$$p(i) = -\ln(1 - i/2^n)/2^n.$$

We carefully choose a threshold p_{th} to cut the distribution, obtaining a renormalized distribution with a flattop to approximate the ideal distribution with different levels of fidelity, as shown in Fig. 3(a). Then, we use the native rejection sampling to produce samples according to this new flattop distribution by repeating the following steps: (1) Suggest a random sample i and calculate its probability $p(i)$. (2) Accept the sample i with the probability of $\min(p(i)/p_{\text{th}}, 1)$. We observe a trade-off between sampling efficiency and sample fidelity, as shown in Fig. 3(b). By setting the threshold to $p_{\text{th}} = 2.4 \times 2^{-n}$, we get the sample fidelity of 0.9 with sampling efficiency of 0.38. That is, the sampler can produce one statistically independent and high-fidelity sample by consuming about three probability amplitudes.

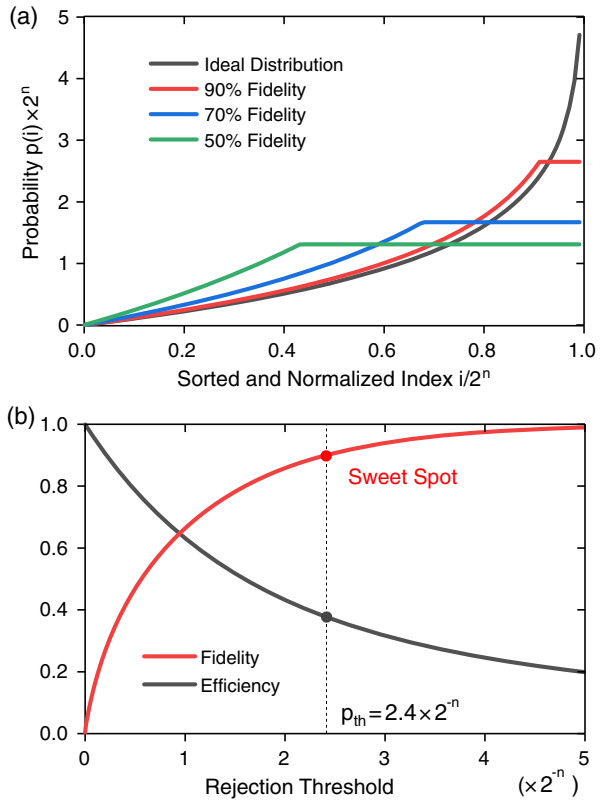

FIG. 3. Threshold rejection sampling protocol. (a) The ideal population distribution of a random quantum state is approximated by cut-peak distributions. Approximate distributions of 0.9, 0.7, and 0.5 fidelity are shown. (b) The trade-off between the sample fidelity and sampling efficiency. A sweet spot of 0.9 sample fidelity and 0.38 efficiency is obtained at a cut-peak threshold of 2.4×2^{-n}.

In the above two steps, we have described how to extend both the scale and the efficiency of classical simulation of quantum sampling. The result is summarized in Fig. 4. A phase transition of classical hardness emerges at the boundary of 49 qubits: we enlarge the classically easy area A of 49 physical qubits barrier to include a new area B of 49 logical qubits. We further note that classical algorithms by mixing Schrödinger and Feynman methods [8] could be used to exploit the trade-off between memory usage and running time to slightly extend the classically easy area.

Our results provide a physically intuitive way to understand the boundary of classical simulation in the similar concepts of quantum teleportation and one-way quantum computing. The concept is helpful to design optimal quantum sampling experiments: design smaller quantum circuits with more logical qubits. For example, one can subtract some of the physical qubits or quantum gates in the circuit, while keeping the logical qubits unchanged, or use nondiagonal entangling gates and nonlocal entangling gates to increase the number of logical qubits, while keeping the circuit size unchanged.

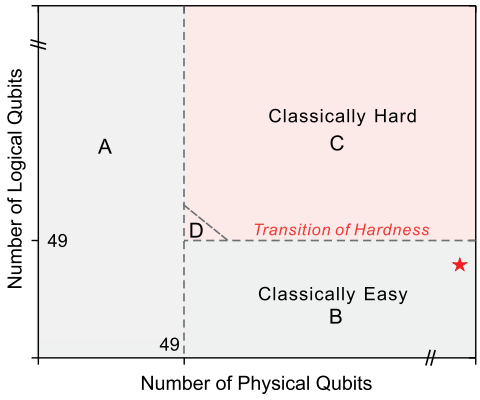

FIG. 4. New 49-qubit barrier. Our protocol extends the classically easy area of random quantum circuit sampling from area A to area B, where the number of physical qubits or logical qubits (proportional to the circuit depth) is smaller than 49. The classically hard quantum sampling is in area C. Around the corner of area C, a small area D may be classically easy by considering the trade-off between memory usage and running time. The star symbol represents the 1000 physical-qubit simulations in this Letter.

In summary, we propose and demonstrate a quantum-inspired algorithm to solve large random quantum circuit sampling. Our protocol uses quantum teleportation to swap the role of space and time in quantum circuits, presenting a new efficient tool to simulate low-depth quantum circuits and, for the first time, extend the versatile quantum concept of teleportation to enhance classical technology.

This work was supported by the National Natural Science Foundation of China, the Chinese Academy of Sciences, the National Fundamental Research Program and the Anhui Initiative in Quantum Information Technologies.

[1] M. A. Nielsen and I. L. Chuang, *Quantum Computation and Quantum Information: 10th Anniversary Edition*, 10th ed. (Cambridge University Press, New York, 2011).
[2] A. W. Harrow, A. Hassidim, and S. Lloyd, Phys. Rev. Lett. **103**, 150502 (2009).
[3] A. Aspuru-Guzik, A. D. Dutoi, P. J. Love, and M. Head-Gordon, Science **309**, 1704 (2005).
[4] R. Barends, J. Kelly, A. Megrant, A. Veitia, D. Sank, E. Jeffrey, T. C. White, J. Mutus, A. G. Fowler, B. Campbell *et al.*, Nature (London) **508**, 500 (2014).
[5] C. J. Ballance, T. P. Harty, N. M. Linke, M. A. Sepiol, and D. M. Lucas, Phys. Rev. Lett. **117**, 060504 (2016).
[6] J. P. Gaebler, T. R. Tan, Y. Lin, Y. Wan, R. Bowler, A. C. Keith, S. Glancy, K. Coakley, E. Knill, D. Leibfried, and D. J. Wineland, Phys. Rev. Lett. **117**, 060505 (2016).
[7] S. Aaronson and A. Arkhipov, in *Proceedings of the Forty-Third Annual ACM Symposium on Theory of Computing* (ACM, New York, 2011), pp. 333–342.
[8] S. Aaronson and L. Chen, arXiv:1612.05903.
[9] A. W. Harrow and A. Montanaro, Nature (London) **549**, 203 (2017).
[10] A. Bouland, B. Fefferman, C. Nirkhe, and U. Vazirani, Nat. Phys. **15**, 159 (2019).
[11] J. Preskill, Quantum **2**, 79 (2018).
[12] S. Boixo, S. V. Isakov, V. N. Smelyanskiy, R. Babbush, N. Ding, Z. Jiang, M. J. Bremner, J. M. Martinis, and H. Neven, Nat. Phys. **14**, 595 (2018).
[13] C. Neill, P. Roushan, K. Kechedzhi, S. Boixo, S. Isakov, V. Smelyanskiy, A. Megrant, B. Chiaro, A. Dunsworth, K. Arya *et al.*, Science **360**, 195 (2018).
[14] A. M. Dalzell, A. W. Harrow, D. E. Koh, and R. L. La Placa, arXiv:1805.05224.
[15] E. Pednault, J. A. Gunnels, G. Nannicini, L. Horesh, T. Magerlein, E. Solomonik, and R. Wisnieff, arXiv:1710.05867.
[16] I. L. Markov and Y. Shi, SIAM J. Comput. **38**, 963 (2008).
[17] S. Boixo, S. V. Isakov, V. N. Smelyanskiy, and H. Neven, arXiv:1712.05384.
[18] Z.-Y. Chen, Q. Zhou, C. Xue, X. Yang, G.-C. Guo, and G.-P. Guo, Sci. Bull. **63**, 964 (2018).
[19] R. Li, B. Wu, M. Ying, X. Sun, and G. Yang, arXiv:1804.04797.
[20] J. Chen, F. Zhang, C. Huang, M. Newman, and Y. Shi, arXiv:1805.01450.
[21] I. L. Markov, A. Fatima, S. V. Isakov, and S. Boixo, arXiv:1807.10749.
[22] B. Villalonga, S. Boixo, B. Nelson, C. Henze, E. Rieffel, R. Biswas, and S. Mandrà, arXiv:1811.09599.
[23] B. Villalonga, D. Lyakh, S. Boixo, H. Neven, T. S. Humble, R. Biswas, E. G. Rieffel, A. Ho, and S. Mandrà, arXiv:1905.00444.
[24] C. H. Bennett, G. Brassard, C. Crépeau, R. Jozsa, A. Peres, and W. K. Wootters, Phys. Rev. Lett. **70**, 1895 (1993).
[25] R. Raussendorf and H. J. Briegel, Phys. Rev. Lett. **86**, 5188 (2001).
[26] J. C. Bridgeman and C. T. Chubb, J. Phys. A **50**, 223001 (2017).
[27] J. Biamonte and V. Bergholm, arXiv:1708.00006.
[28] See Supplemental Material at http://link.aps.org/supplemental/10.1103/PhysRevLett.124.080502 for the layouts of qubits and entangling gates, the 3D layouts of logical qubits, and the calculation of sampling efficiency.
[29] A. Kandala, A. Mezzacapo, K. Temme, M. Takita, M. Brink, J. M. Chow, and J. M. Gambetta, Nature (London) **549**, 242 (2017).
[30] J. Emerson, Y. S. Weinstein, M. Saraceno, S. Lloyd, and D. G. Cory, Science **302**, 2098 (2003).
[31] Y. S. Weinstein, W. G. Brown, and L. Viola, Phys. Rev. A **78**, 052332 (2008).
[32] H. Fu, J. Liao, J. Yang, L. Wang, Z. Song, X. Huang, C. Yang, W. Xue, F. Liu, F. Qiao *et al.*, Sci. Chin. Inf. Sci. **59**, 072001 (2016).
[33] A. Neville, C. Sparrow, R. Clifford, E. Johnston, P. M. Birchall, A. Montanaro, and A. Laing, Nat. Phys. **13**, 1153 (2017).